Corrosion Science 102 (2016) 317–325

Contents lists available at ScienceDirect

Corrosion Science

journal homepage: www.elsevier.com/locate/corsci

Corrosion of thin, magnetron sputtered Nb_2O_5 films

Marina Fuser Pillis[a], Guilherme Altomari Geribola[a], Guilherme Scheidt[a], Edval Gonçalves de Araújo[b], Mara Cristina Lopes de Oliveira[c], Renato Altobelli Antunes[d,*]

[a] Instituto de Pesquisas Energéticas e Nucleares (IPEN/CNEN-SP), Centro de Ciência e Tecnologia de Materiais (CCTM), 05508-000 São Paulo, SP, Brazil
[b] Departamento de Engenharia Mecânica, Universidade Federal de Pernambuco (UFPE), 50670-901 Recife, PE, Brazil
[c] Electrocell Ind. Com. Equip. Elet. LTDA, Centro de Inovação, Empreendedorismo e Tecnologia (CIETEC), 05508-000 São Paulo, SP, Brazil
[d] Centro de Engenharia, Modelagem e Ciências Sociais Aplicadas (CECS), Universidade Federal do ABC (UFABC), 09210-580 Santo André, SP, Brazil

ARTICLE INFO

Article history:
Received 17 May 2015
Received in revised form 4 October 2015
Accepted 16 October 2015
Available online 23 October 2015

Keywords:
Sputtered films
RBS
EIS
Oxide coatings

ABSTRACT

Niobium oxide based thin films were deposited on AISI 316 stainless steel substrates using reactive DC magnetron sputtering. Structure, composition and corrosion resistance of the niobium oxide films were studied. The corrosion behavior of the specimens was evaluated by electrochemical impedance spectroscopy (EIS) and potentiodynamic polarization. The concentration of niobium and oxygen in the films was obtained by Rutherford backscattering spectroscopy (RBS). The film structure was analyzed by X-ray diffractometry. The corrosion resistance of the substrate was improved by the Nb_2O_5 layers. The best protective performance was achieved for the deposition time of 15 min.

1. Introduction

Niobium oxide films have attracted much attention in materials science in the past few years. NbO, NbO_2 and Nb_2O_5 are the most stable phases, being niobium pentoxide the one with the lowest Gibbs free energy of formation between them and, hence, the most thermodynamically favorable to form [1]. The growing interest in Nb_2O_5 arises from its applicability in several advanced devices such as sensors, solar cells, capacitors and smart windows [2–4]. In these devices electronic and optical properties of Nb_2O_5 films such as photoelectric and photocatalytic activity, high permittivity, high refractive index and transparency in the UV–vis–NIR region have been advantageously exploited to produce a variety of optical devices [5,6]. Furthermore, high wear resistance, good thermal stability and biocompatibility have been reported as attributes that widen the engineering applications of Nb_2O_5 layers to additional areas such as biomedical devices [7] and barrier coatings [8].

In addition to the above-mentioned properties, corrosion resistance is a must-attend issue of metallic-coated surfaces in engineering applications [9]. Some reports reveal the good corrosion protection ability of Nb_2O [10,11].

Several deposition techniques can be used to produce niobium-based coatings. Sol–gel techniques, chemical vapor deposition (CVD) and physical vapor deposition (PVD) methods have been reported [12–14]. The anti-corrosion performance of coatings produced by PVD is markedly affected by deposition parameters [15]. The development of PVD-based Nb_2O_5 coatings with enhanced corrosion properties can be more promptly accomplished if the correlation between coatings structure and deposition parameters is known. However, scientific investigations devoted to the study of this correlation are lacking in the literature. The present work investigates the relationship between film structure, electrochemical behavior and deposition time of Nb_2O_5 films produced by DC magnetron sputtering.

2. Experimental

2.1. Substrate preparation and film deposition

The substrates for the present investigation were AISI 316 stainless steel circular samples with a diameter of 19 mm and 6 mm-thick. The samples were ground up to 600 grit using SiC paper. The surface was degreased with acetone and thoroughly washed with distilled water, then dried in a hot air stream prior to deposition. These samples were used for the electrochemical characterization. Silicon (1 0 0) plates were used as substrates

* Corresponding author.
E-mail address: renato.antunes@ufabc.edu.br (R.A. Antunes).

http://dx.doi.org/10.1016/j.corsci.2015.10.023
0010-938X/

for Rutherford backscattering spectroscopy (RBS), X-ray diffractometry (XRD), scanning electron microscopy (SEM) and also for thickness measurements by ellipsometry.

Niobium oxide films were produced by reactive DC magnetron sputtering from a niobium target (99.9% purity) in $Ar + O_2$ atmosphere. The oxygen content was kept constant during deposition and was relatively high to yield Nb_2O_5 films with composition close to the stoichiometric composition [16]. Deposition was performed at room temperature. Two different deposition times were tested: 15 min and 30 min. The pressure in the chamber was constant and kept at 8.40×10^{-2} Pa. The distance between target and substrate was 15 cm and the direct current (DC) power was 400 W. Argon and oxygen flows were 100 mL min^{-1} and 15 mL min^{-1}, respectively.

2.2. Film characterization

The atomic fractions of niobium and oxygen in the films were obtained by RBS. The analyses were made using a helium beam of energy 2.2 MeV in an electrostatic accelerator of type Pelletron-tandem, model 5SDH with a detection angle of 120°. Film thickness was determined using ellipsometry. The measurements were performed using a Rudolph Research Corporation ellipsometer, model Auto EL IV MS with incident angle of 70° and wavelength of 632.8 nm. A field emission-scanning electron microscope (FEG-SEM) FEI Quanta 600 was used to observe the cross-sections of the niobium oxide films with regard to film thickness and compactness.

Film structure was determined using XRD analysis. The measurements were carried out in Philips X'Pert equipment using Cu-Kα radiation in glancing angle mode with incident angle of 5° in the range 20–80° with step size of 0.02°.

The electrochemical behavior of deposited films was evaluated by EIS and potentiodynamic polarization curves using a potentiostat/galvanostat Autolab PGSTAT 100 equipped with FRA (frequency response analyser) module. The electrolyte consisted of naturally aerated NaCl 3.5 wt.% solution at room temperature. The test setup was comprised of a conventional three-electrode cell. Pure platinum wire (diameter of 0.5 mm) was used as counter-electrode, a saturated calomel electrode (SCE) as reference and the niobium oxide-coated sample as working electrode. Three different samples of each condition were tested to ensure reproducibility. The samples remained immersed for 19 days before the tests in order to achieve a steady state condition for the electrochemical measurements. Initially, the open circuit potential was monitored for 1 h. Next, EIS measurements were carried out at the open circuit potential in the frequency range from 100 kHz to 10 mHz. The amplitude of the excitation signal was set to 10 mV (rms) with an acquisition rate of 10 points per decade. Following the EIS measurements, the samples were submitted to potentiodynamic polarization starting at $-0.25\,V_{SCE}$ versus the open circuit potential and stopping at $+1.0\,V_{SCE}$ at a scanning rate of 1 mV s^{-1}. After polarization, the electrodes were rinsed with deionized water and the pits formed on the surface were measured by using confocal laser scanning microscopy (CLSM) (Olympus LEXT OLS4100). The five deepest pits were measured on each sample in order to give a representative indication of the pitting corrosion resistance. SEM micrographs of the top surfaces were obtained before immersion and after the polarization tests using a TM3000 Hitachi scanning electron microscope.

3. Results and discussion

3.1. Structure, thickness and composition

Fig. 1 shows the RBS spectra of the films produced with deposition times of 15 min and 30 min at room temperature. The spectra

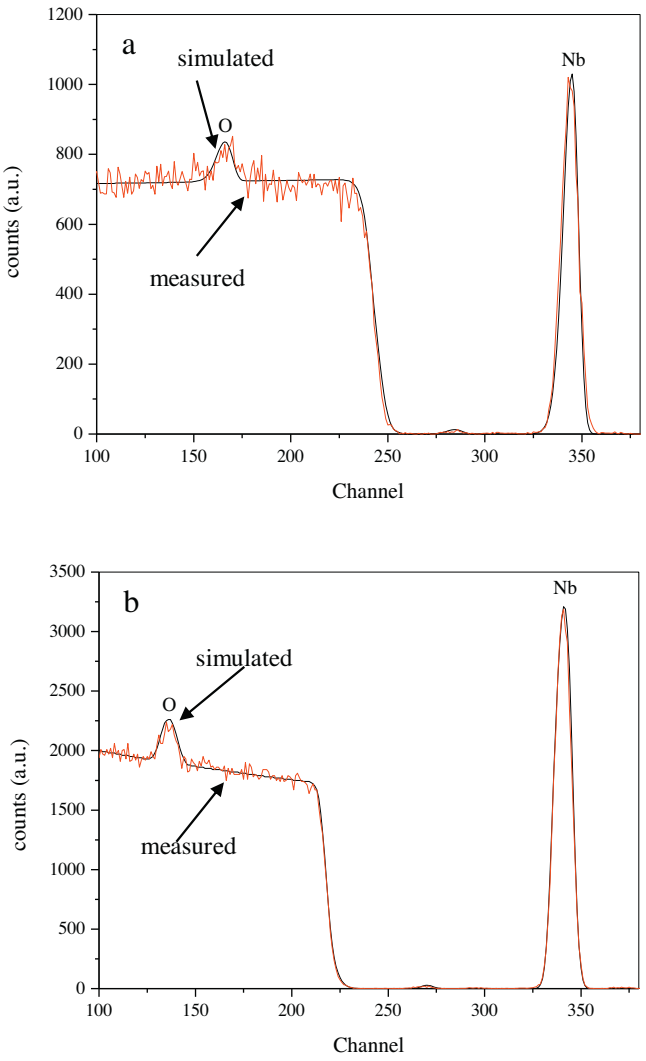

Fig. 1. RBS spectra of the niobium oxide films produced with different deposition times at room temperature: (a) 15′; (b) 30′.

were fitted using the software SIMRA [17]. The stoichiometry of the deposited coatings was determined for a fixed oxygen flow of 15 mL min^{-1}. The Nb/O ratio was found to be 0.3738 for both films, independently of the deposition time. The RBS measurements indicate that the films stoichiometry is $Nb_2O_{5.35}$ which is close to Nb_2O_5. Small amounts (1.5%) of argon were also found in the films probably due to incorporation of the argon ions employed to sputter the niobium target [16]. Ramírez et al. [10] have found an Nb/O ratio within the range 0.39–0.43 for niobium oxide films through RBS. Serényi et al. [18] have found the compound $Nb_2O_{5.14}$ with Nb/O ratio of 0.3891 for niobium oxide sputtered films. The work by Foroughi-Abari and Cadien [19] showed that the nature of the niobium oxide formed during DC magnetron sputtering deposition depends on the oxygen flow. NbO, NbO_2 and Nb_2O_5 have been obtained at oxygen flow rates of 2, 4 and 6 mL min^{-1}, respectively. The results expressed here are in agreement with the literature and show that the deposition time did not influence the stoichiometry of the niobium oxide films.

Ellipsometric measurements have shown that the film thickness increased with deposition time. In fact, the thickness increased from 36 nm to 70 nm when the deposition was raised from 15 to 30 min. FEG-SEM cross-sectional views of the niobium oxide films obtained for the deposition times of 15 and 30 min confirmed this finding as shown in Fig. 2. The increase of PVD film thickness with

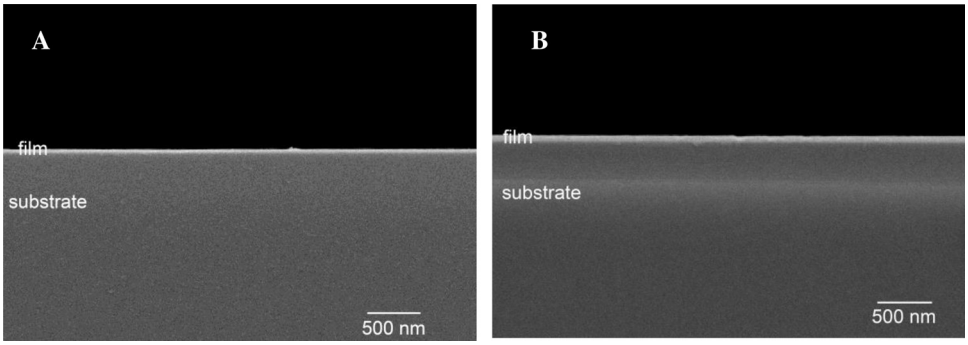

Fig. 2. FEG-SEM cross-sectional views of the niobium oxide films obtained for different deposition times: (A) 15 min; (B) 30 min.

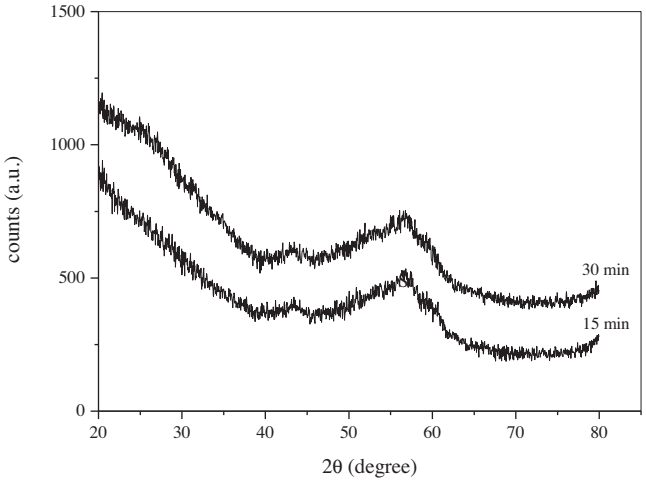

Fig. 3. XRD patterns of Nb_2O_5 films obtained at different deposition times.

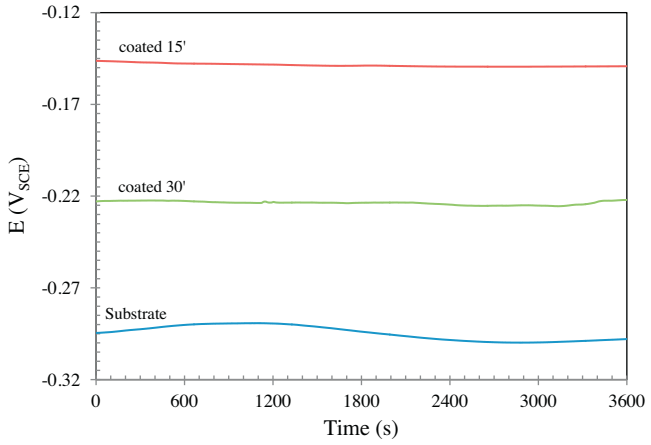

Fig. 4. Open circuit potential versus time for the uncoated and Nb_2O_5-coated 316 stainless steel.

deposition is expected and has been reported by other authors [20]. Thicker coatings may improve the corrosion resistance of metallic substrates due to the longer diffusion path of aggressive species [21].

XRD patterns of the deposited films are shown in Fig. 3. No reflections can be observed. It is clear that the Nb_2O_5 films have an amorphous character. This is in good agreement with the results published by other authors [10,18]. The amorphous nature of oxide films can be advantageously explored to improve the corrosion resistance of metallic materials. It is reported that corrosion resistance should increase for amorphous surfaces in comparison to crystalline counterparts due to the lack of crystalline defects such as grain boundaries and dislocations as well as due to chemical homogeneity and layer compactness [22].

3.2. Corrosion behavior

3.2.1. Open circuit potential monitoring and electrochemical impedance spectroscopy

Initially, the open circuit potential (OCP) was monitored for 1 h in order to ensure a steady state for the EIS measurements. Fig. 4 shows the plots of OCP versus time for the bare 316 stainless steel substrate and for the Nb_2O_5-coated specimens. The OCP of the substrate is more negative than that of the coated specimens, suggesting that its surface is more prone to corrosion processes in comparison with the coated substrate. As observed in Fig. 4, a steady state condition was achieved after monitoring. Thus, EIS measurements were carried out at the open circuit potential obtained at the end of the monitoring period.

The Nyquist plots of the niobium oxide films obtained after 19 days of immersion in 3.5 wt.% NaCl solution at room temperature are shown in Fig. 5A. The plot obtained for the uncoated substrate is also shown for comparison. The inset displays the expanded view of the Nyquist plots in order to more clearly realize the different EIS responses of the coated and uncoated substrates.

The plots of the niobium oxide-coated substrate are characterized by one capacitive loop, independently of the deposition time. The radii of the capacitive loops are much larger for the coated material than for the bare substrate. Corrosion resistant surfaces are associated with high impedance values at low frequencies which correspond to less flattened capacitive loops with large radius [23]. The small capacitive loop of the uncoated substrate denotes its lower corrosion resistance when compared to the niobium oxide coated samples.

The EIS response of the coated and uncoated substrates was also assessed by Bode phase angle plots (Fig. 5B). The plots of the coated samples have a wide plateau extending from approximately 1 kHz up to 0.01 Hz. The plateau reaches −80° at its maximum and then decreases to −70° at the lowest frequencies. For the uncoated substrate the phase plot is also characterized by a plateau near −80°. However, it is shorter than the plateau observed for the niobium oxide coated samples, beginning at approximately 10 Hz, extending up to 0.01 Hz. It is known from the literature that a pure capacitive response of the electrode surface would give a phase angle of −90°. The more the phase angle deviates from this value, the more imperfect is the capacitive behavior of the electrode surface [24]. The phase plots in Fig. 4b also indicate that the coated samples respond to the sinusoidal perturbation signal at higher frequencies than the uncoated substrate which is a typical EIS response of coated metals

[25]. Drop off of the phase angle at low frequencies has been associated with decreased corrosion resistance due to charge transfer reactions at the electrode/electrolyte interface at the base of the defects of coated metals [26]. This behavior was not observed in the present work regarding the EIS response of the niobium oxide-coated samples. The phase angles formed a stable plateau up to the lowest frequencies, indicating the stability of these films throughout the test. The high impedance values observed at the lowest frequencies (Fig. 5A) also confirm this hypothesis. Bode plots showing the variation of the impedance modulus with frequency are also

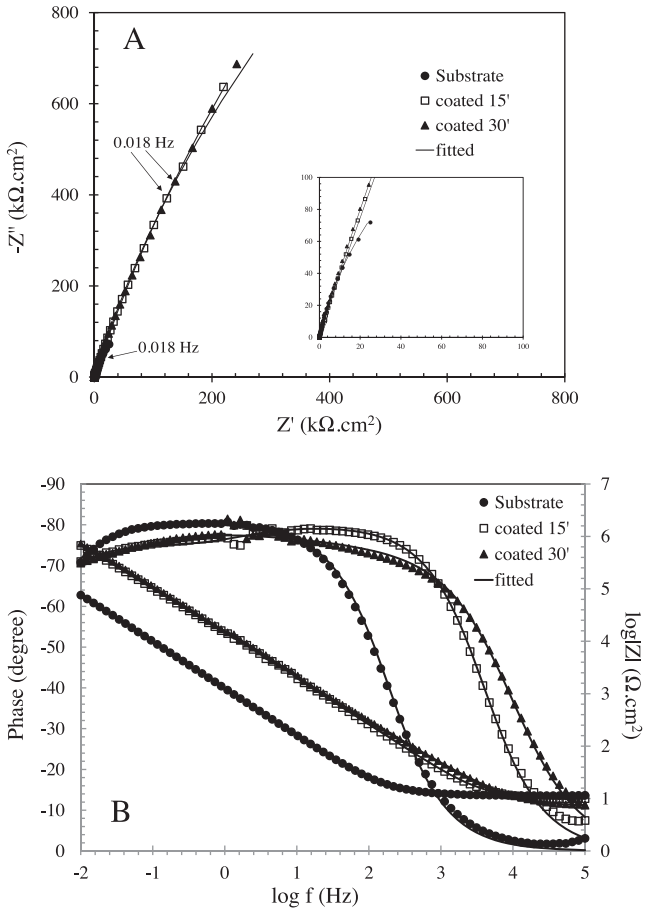

Fig. 5. (A) Nyquist and (B) phase plots of the niobium oxide coated and uncoated substrates obtained after 19 days of immersion 3.5 wt.% NaCl solution at room temperature.

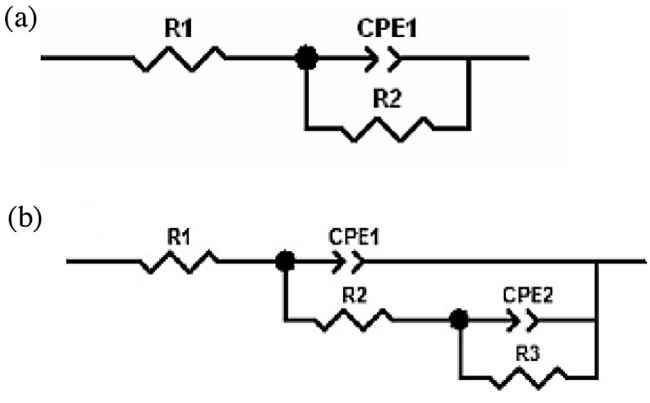

Fig. 6. ECs used to simulate the EIS experimental data: (a) uncoated 316 stainless steel; (b) niobium-oxide coated 316 stainless steel.

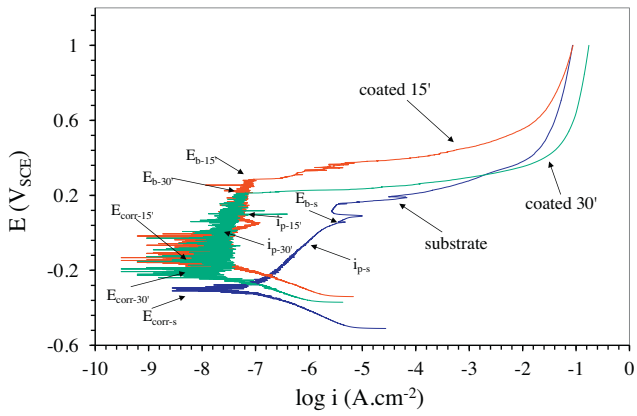

Fig. 7. Potentiodynamic polarization curves of the niobium coated and uncoated substrates obtained after 19 days of immersion 3.5 wt.% NaCl solution at room temperature.

shown in Fig. 5B. The high impedance of the coated specimens is clearly seen in comparison with the bare substrate.

A more quantitative interpretation of the EIS data was obtained by fitting the experimental results using equivalent circuits (ECs). The EC used to simulate the EIS response of the bare substrate is shown in Fig. 6a. This circuit consists of only one time constant to model the corrosion processes occurring at the electrolyte/metal interface and has been used by several authors to represent the electrochemical behavior of uncoated stainless steels in NaCl solutions [27,28]. A constant phase element (CPE) is used instead of a pure capacitor to account for the heterogeneity of the electrode [29]. In this circuit R_1 denotes the electrolyte resistance, CPE_1 models the pseudocapacitance of the double layer at the electrolyte/metal interface and R_2 is the charge transfer resistance of the metallic surface. The impedance of a CPE (Z_{CPE}) is defined as shown in Eq. (1).

$$Z_{CPE} = [Q(j\omega)^n]^{-1} \quad (1)$$

In this equation Q is the magnitude of the CPE and n its exponent. For pure capacitors $n = 1$ and $n = 0.5$ for diffusion controlled processes. The angular frequency is ω and $j = \sqrt{-1}$ [30]. For the niobium oxide-coated samples the best fitting was given by the circuit shown in Fig. 6b. Two time constants are used to model the response of the coated substrate. This circuit is often employed to simulate EIS data obtained from coated metals [31–33]. Ramírez et al. [14] have also used this circuit to simulate EIS experimental data obtained for PVD niobium oxide-based films deposited on stainless steel substrates. In this circuit, R_1 is the electrolyte resistance, CPE_1 is associated with the capacitance of the niobium oxide-based coating and R_2 is the coating resistance which is influenced by the presence of defects such as flaws and pores. The low frequency time constant is used to model the electrochemical response at the base of the coating defects, accounting for the electrolyte/substrate interface. CPE_2 is associated with the double layer capacitance and R_3 models the charge transfer resistance. The parameters obtained by the fitting procedure are shown in Table 1.

According to Ramírez et al. [14], the protective nature of coatings is related to the values of both R_2 and R_3, scaling up with them. The data shown in Table 1 expresses much higher values of charge transfer resistance for the coated sample in comparison the uncoated one, thus indicating that the corrosion resistance of the stainless substrate was significantly improved by the niobium oxide films. However, the relatively low values of R_2 for the coated samples imply that the films are not immune to electrolyte penetration through coating defects. The film obtained at 15 min of deposition presented a better response than the film obtained

Table 1
EIS fitting parameters for the bare 316 stainless steel substrate and coated with Nb_2O_5 films.

Sample	R_1 ($\Omega\,cm^2$)	Q_1 ($10^{-4}\,F\,cm^{-2}\,s^{\alpha-1}$)	n_1	R_2 ($k\Omega\,cm^2$)	Q_2 ($10^{-5}\,F\,cm^{-2}\,s^{\alpha-1}$)	n_2	R_3 ($k\Omega\,cm^2$)
Coated 15 min	10	0.13	0.89	118	0.27	0.70	8480
Coated 30 min	7	0.30	0.78	137	2.09	0.97	3830
Substrate	12	1.52	0.89	482	–	–	–

at 30 min, suggesting that the corrosion resistance was adversely affected when the coating thickness increased from 36 nm (at 15 min) to 70 nm (30 min). High capacitance values are associated with a lower corrosion resistance, being related to increased area exposed to the electrolyte due to a more defective coating layer [31,34]. The capacitance associated with the 15 min-coating is lower than that for the 30 min-coating, confirming the more efficient barrier property obtained for the first film. Coating thickness is known to influence the corrosion behavior of metallic substrates. Depending on the density and defects formed on the protective film, increasing thicknesses can be beneficial [35,36] or even decrease the corrosion resistance [37,38] of the underlying metal surface. Berasategui et al. [39], for instance, reported that the corrosion resistance of aluminum-doped ZnO (AZO) sputtered films increased with thickness. This improved protection ability was attributed to the film morphology. The thicker layer presented bigger grain sizes than thinner one with less grain boundaries. A similar effect was reported by Surmeneva et al. [35] for sputtered hydroxyap-

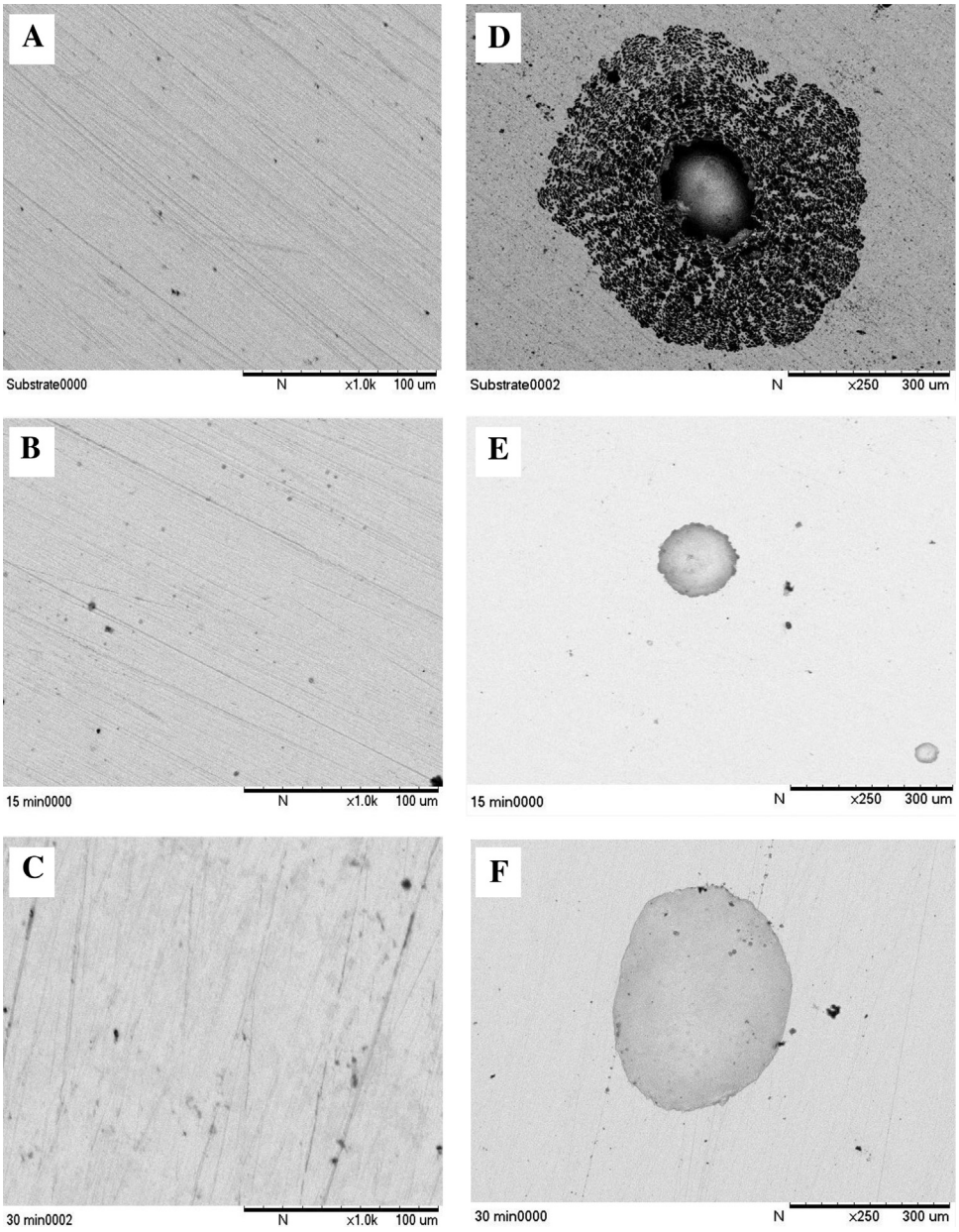

Fig. 8. SEM micrographs of the top surfaces of the uncoated and Nb_2O_5-coated 316 stainless steel samples: (A) uncoated substrate, before immersion; (B) 15′-coated sample, before immersion; (C) 30′-coated sample, before immersion; (D) uncoated substrate, after polarization; (E) 15′-coated sample, after polarization; (F) 30′-coated sample, after polarization.

atite layers. Conversely, increasing film thickness can also impair the corrosion resistance of the coated substrate. This effect was recently reported by Liu et al. [40]. These authors evaluated the corrosion behavior of sputtered cerium oxide based coatings with different thickness on an aluminum alloy substrate. Increasing the coating thickness led to reduced corrosion protection ability to the higher porosity and defects in the film layer. Sonmez et al. [41] observed that thicker hydroxyapatite layers obtained by dip coating presented more cracks than thinner layers, depressing the corrosion resistance. The detrimental effect of increasing coating thickness due to the development of more cracks on the surface layer was also reported by Zhuang et al. [42] for Cr-doped diamond like carbon films deposited by cathodic arc processes. Our results point to a detrimental effect of the coating thickness on the overall corrosion behavior of the niobium oxide-coated substrate. Since our Nb_2O_5 films presented an amorphous character according to the results obtained by XRD (Fig. 3), grain size effects can be neglected. As-deposited Nb_2O_5 films are usually amorphous [43] but can crystallize depending on annealing treatments employed after deposition [44]. After crystallization, grain sizes are formed and the surface roughness increases [45]. The corrosion resistance can, therefore, be depressed by crystallization [46]. However, these effects are not encountered in the present work due to the amorphous nature of the as-deposited films. In the same regard, film morphology and porosity can affect the corrosion resistance of coated metals. Both aspects have been considered to explain the results obtained here, as described in Section 3.2.2.

Comparing our results with those obtained by Ramírez et al. [14] reveal that the best niobium oxide film produced by these authors has lower capacitance and higher resistance than our 15 min-coating, according to EIS measurements. However, the films obtained by Ramírez et al. were 200 nm-thick whereas our 15 min-film is only 36 nm-thick. Hence, the very thin niobium-oxide layer produced in this work provided an efficient barrier against corrosion of the 316 stainless steel substrate. This result has interesting implications for engineering purposes, since it points to a great enhancement of the corrosion resistance at a relatively short deposition time. In order to gain a more clear understanding on the correlation between film structure and the corresponding corrosion behavior, additional analyses were carried out, as described in the next section.

3.2.2. Potentiodynamic polarization curves

The corrosion behavior of the niobium oxide coated substrate was further assessed using potentiodynamic polarization curves. The results are shown in Fig. 7. The values of corrosion potential (E_{corr}) and corrosion current density (i_{corr}) obtained from these curves are displayed in Table 2. The values of i_{corr} were determined using the Tafel extrapolation method, considering only the cathodic branch of the polarization curve. This methodology was followed based on the fact that the passive regions in the polarization curves makes difficult to accurately determine the anodic Tafel slope and, thus, the corrosion current density can be suitably determined by extrapolating only the cathodic branch [47,48]. The values for breakdown potential (E_b) and passive current density (i_p) are also displayed. The values of i_p were determined from the middle of the passive region, as proposed by Ningshen et al. [49].

The curve of the uncoated substrate is typical of passive metals showing an incipient passive region in the anodic branch that extends through approximately 240 mV_{SCE} from up to a first breakdown at 36 mV_{SCE}. Stainless steel substrates are prone to pitting corrosion and the breakdown potential indicates its onset. Final breakdown is seen at approximately 150 mV_{SCE} as indicated by the sharp increase of the current density. The polarization curves of the niobium oxide-coated substrates are also typical of passive surfaces. This can be promptly realized by the presence of an approximately constant current density region in the anodic branches of the curves. It is also noteworthy that the passive behavior of the coated samples is more stable than that of the uncoated substrate, since the current density in the passive region is clearly lower than that in the polarization curve of the bare sample, as also indicated in Table 2. Moreover, the breakdown potentials are higher for the coated samples, indicating improved resistance to the nucleation and growth of corrosion pits. Hence, the presence of the Nb_2O_5 films strongly affected the anodic behavior of the 316 substrate. Notwithstanding, the values of b_c for the coated samples are similar to that for the bare substrate, indicating that the cathodic reactions were slightly affected by the presence of the Nb_2O_5 films.

From Table 2 it is observed that the values of E_{corr} were shifted to more anodic potentials in the presence of the niobium oxide coatings. This is associated with more corrosion resistant surfaces. Following this trend, the values of i_{corr} are lower for the coated samples than for the uncoated one, thus indicating that the corrosion processes proceed at a slower rate at these surfaces. These

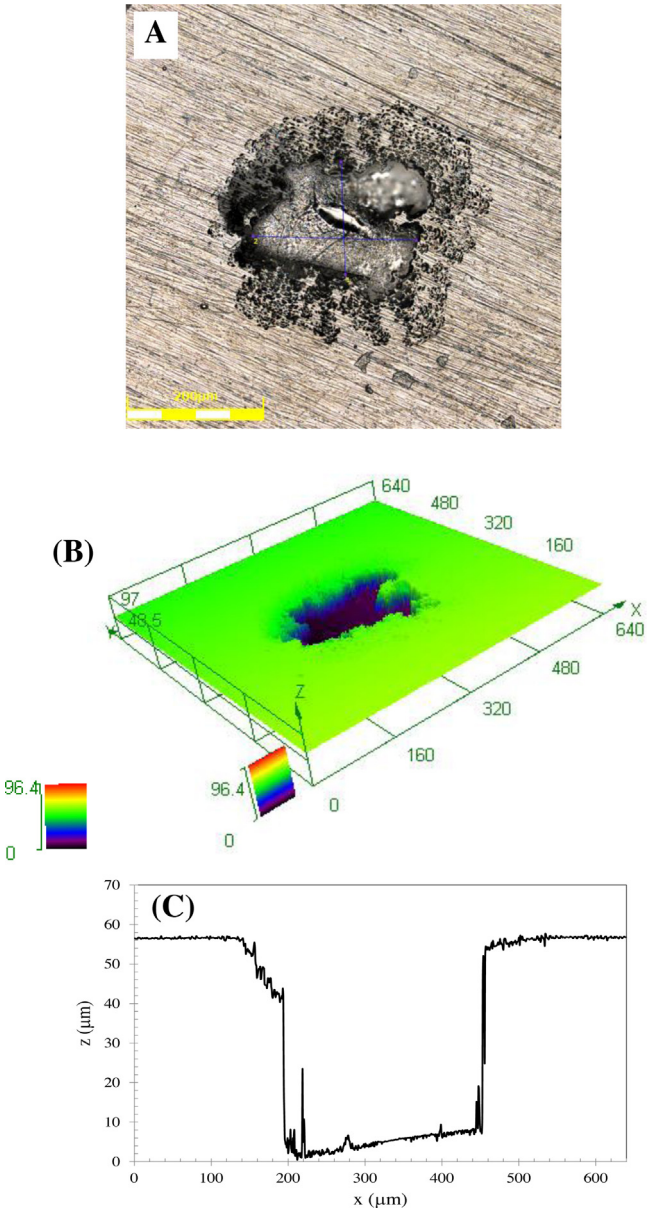

Fig. 9. CSLM images of corrosion pit formed on the surface of uncoated 316 stainless steel sample: (A) 2D-image; (B) 3D-image; (C) transverse profile.

Table 2
Electrochemical parameters of the bare 316 stainless steel substrate and coated with Nb_2O_5 films.

Condition	i_{corr} ($\mu A\,cm^{-2}$)	E_{corr} (V_{SCE})	b_c (mV/decade)	i_{pass} ($\mu A\,cm^{-2}$)	E_b (V_{SCE})
Coated 15′	0.042	−0.149	−88	0.05	0.282
Coated 30′	0.036	−0.222	−98	0.02	0.210
Substrate	0.112	−0.298	−97	0.91	0.081

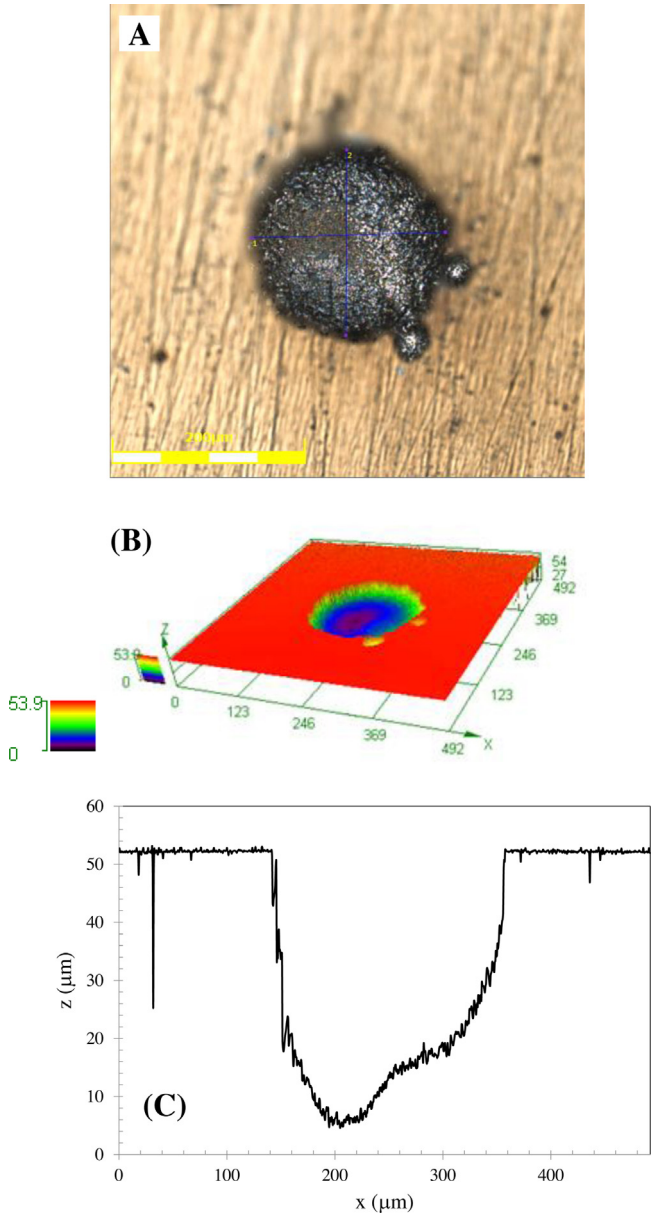

Fig. 10. CSLM images of corrosion pit formed on the surface of 15 min-coated sample: (A) 2D-image; (B) 3D-image; (C) transverse profile.

results reveal that the niobium oxide films have a strong barrier effect against corrosion which is active even after 19 days of immersion, confirming the data obtained by EIS. The beneficial effect of niobium oxide-based films to the corrosion resistance of metallic substrates has been observed by other authors [14]. The amorphous nature of the films (Fig. 3) can contribute to enhance the protective character of the Nb_2O_5 films observed in the present work.

The surface morphology of the uncoated and Nb_2O_5-coated substrate was assessed by SEM. Fig. 8 shows the SEM micrographs obtained before and after the polarization tests for the uncoated and Nb_2O_5-coated samples. The top surfaces of the samples are mostly featureless. The presence of the thin Nb_2O_5 amorphous layers does not allow one to indicate visual differences between the uncoated and coated substrate before the polarization tests, as depicted in Fig. 8A–C. However, the beneficial effect of the Nb_2O_5 films can be perceived when the top surfaces are observed after the polarization tests. The pits formed on the uncoated substrate are bigger than those formed on the coated samples. This is clearly seen by comparing Fig. 8D to Fig. 8E and F.

Our results reveal that is unlikely that the film morphology could have affected the corrosion behavior of the Nb_2O_5-coated samples, since the SEM micrographs obtained before the electrochemical tests did not show any visual differences between each deposition condition and the bare metallic surface. In this respect, we have determined the coating porosity using the EIS data, according to the methodology described in [50,51]. Film porosity (P) can be determined using Eq. (2), where $R_{p,s}$ is the polarization resistance of the uncoated substrate and R_p is the polarization resistance of the coated specimen.

$$P\% = \left(\frac{R_{p,s}}{R_p}\right) \times 100 \quad (2)$$

The charge transfer resistance (R_{ct}) at low frequency corresponds to the polarization resistance and, therefore, film porosity can be estimated from the EIS data shown in Table 1. Thus, using the value of R_2 for polarization resistance of the uncoated substrate and R_3 for the coated samples, the porosity percentage was determined as 5.68% for the 15 min-coating and 12.58% for the 30 min-coating according to Eq. (2). The lower porosity percentage of the 15 min-coating would, therefore, be responsible for its superior corrosion resistance.

After the polarization tests, the corrosion pits formed on uncoated and niobium oxide-coated samples were analyzed by confocal laser scanning microscopy (CLSM). This technique is a powerful tool to characterize the pitting corrosion behavior of metallic materials. Pujar et al. [52] used CLSM to evaluate pit depth in 9Cr–1Mo steel with boron addition. Fernández-Domene et al. [53] characterized the pitting corrosion morphology on a highly-alloyed austenitic stainless steel (UNS N08031) by CLSM. Leiva-García et al. [54] employed CLSM to determine pit profile on the duplex stainless steel UNS 1.4462. Cui et al. [55] measured the pit profile on 304 stainless steel samples submitted to laser surface melting using CLSM. In all these reports, CLSM gave reliable information about the pitting corrosion process. Up to our knowledge, though, CLSM has not been employed by other authors to evaluate the pitting corrosion behavior in niobium oxide-coated metals.

Fig. 9 shows a representative pit formed on the surface of the uncoated 316 stainless steel substrate after the polarization test. A 2D-image is shown in Fig. 9A and a 3D-image is presented in Fig. 9B. Fig. 9C shows the transverse profile of this pit which was used to quantify its depth. Similarly, Figs. 10 and 11 bring the same information for the 15 min-coating and 30 min-coating, respectively. The pits formed on the uncoated substrate have an irregular shape and spread out laterally. In contrast, the pits formed on the niobium oxide coated samples are more regular shaped. Moreover, CLSM analysis allowed determining pit volume and dimensions as shown in Table 3. The results point to a reduced pit maximum volume and maximum depth for the niobium-coated samples in comparison

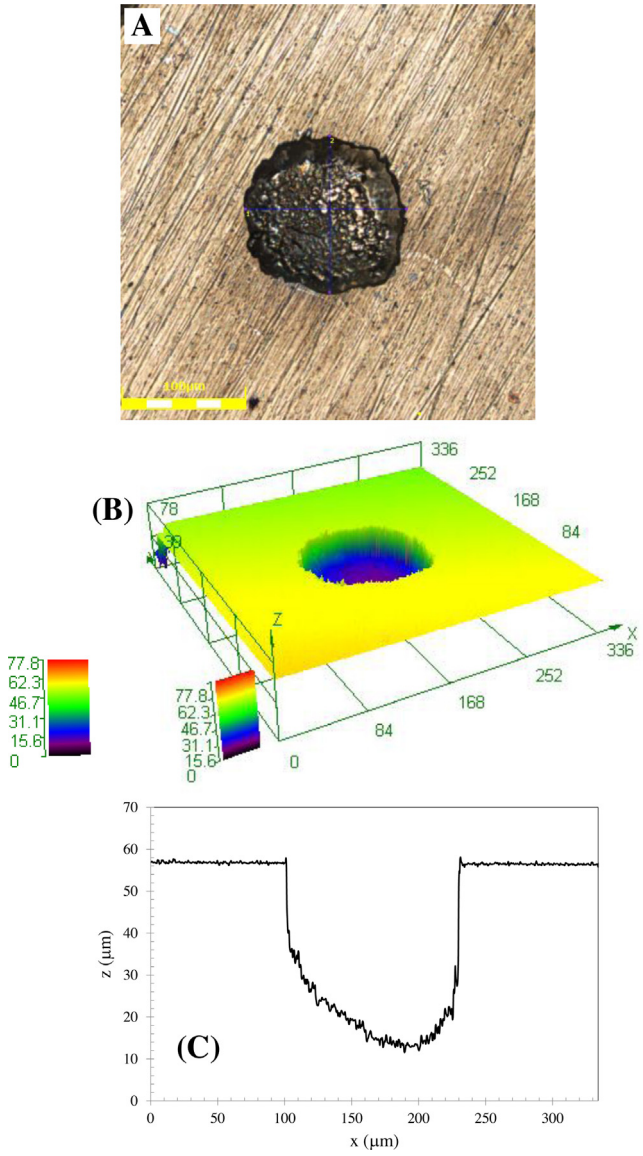

Fig. 11. CSLM images of corrosion pit formed on the surface of 30 min-coated sample: (A) 2D-image; (B) 3D-image; (C) transverse profile.

Table 3
Pit maximum volume and maximum depth obtained from CSLM analysis of pits formed on the bare and Nb_2O_5-coated 316 stainless steel substrate.

Condition	Pit maximum volume (10^6 μm^3)	Maximum depth (μm)
Coated 15 min	0.76 ± 0.31	42.7 ± 8.2
Coated 30 min	1.72 ± 0.40	54.0 ± 4.8
Substrate	3.35 ± 1.04	64.1 ± 10.4

with the bare substrate. The 15 min-coating presented the smallest pits.

The corrosion behavior of the stainless steel substrate was not improved when the deposition time increased from 15 min to 30 min. This result is very interesting from an industrial viewpoint, as the films produced using the lowest deposition time provided a similar corrosion resistance to the one obtained using the longest deposition time. In this context, a shorter deposition process would produce Nb_2O_5 films with equivalent structure and improved corrosion performance and should preferred for real engineering applications.

4. Conclusions

The composition of the niobium oxide films obtained by DC magnetron sputtering was approximately Nb_2O_5 either for the deposition time of 15 min or 30 min, obtaining amorphous coatings in the as-deposited condition. The coating thickness increased with deposition time, being 36 nm for the film obtained at 15 min-deposition and 70 nm for the film obtained at 30 min. Both films increased the corrosion resistance of the 316 stainless steel substrate. However, the corrosion current density increased with the coating thickness and charge transfer resistance decrease. This effect was attributed to the increment of film porosity. Pitting corrosion resistance was also increased for the Nb_2O_5-coated material. The bare metallic specimen presented larger pits and lower breakdown potential than the coated specimens. The film obtained at 15 min provided the most efficient protective layer against localized corrosion.

Acknowledgments

Authors would like to thank Prest Vácuo LTDA, CBMM, IFUSP, EPUSP and CAPES. Olandir Vercino Correa (IPEN/CNEN-SP) is kindly acknowledged for the SEM micrographs of the top surfaces.

References

[1] K.T. Jacob, C. Shekhar, M. Vinay, Thermodynamic properties of niobium oxides, J. Chem. Eng. Data 55 (2010) 4854–4863.
[2] A. Pawlicka, M. Atik, M.A. Aegerter, Synthesis of Nb_2O_5 films for electro-chromic devices, J. Mater. Sci. Lett. 14 (1995) 1568–1570.
[3] R. Jose, V. Thavasi, S. Ramakrishna, Metal oxides for dye-sensitized solar cells, J. Am. Ceram. Soc. 22 (2009) 289–301.
[4] Y.D. Wang, L.F. Yang, Z.L. Zhou, Y.F. Li, X.H. Wu, Effects of calcining temperature on lattice constants and gas-sensing properties of Nb_2O_5, Mater. Lett. 49 (2001) 277–281.
[5] K. Lazarova, M. Vasileva, G. Marinov, T. Babeva, Optical characterization of sol–gel derived Nb_2O_5 thin films, Opt. Laser Technol. 58 (2014) 114–118.
[6] X. Xiao, G. Dong, C. Xu, H. He, H. Qi, Z. Fan, J. Shao, Structure and optical properties of Nb_2O_5 sculptured thin films by glancing angle deposition, Appl. Surf. Sci. 255 (2008) 2192–2195.
[7] P. Amaravathy, S. Sowndarya, S. Sathyanarayanan, N. Rajendran, Novel sol gel coating of Nb_2O_5 on magnesium alloy for biomedical applications, Surf. Coat. Technol. 244 (2014) 131–141.
[8] M. Mazur, M. Szymanska, D. Kaczmarek, M. Kalisz, D. Wojcieszak, J. Domaradzki, F. Placido, Determination of optical and mechanical properties of Nb_2O_5 thin films for solar cells applications, Appl. Surf. Sci. 301 (2014) 63–69.
[9] E.O. Olakanmi, M. Doyoyo, Laser-assisted cold-sprayed corrosion-and wear-resistant coatings: a review, J. Therm. Spray Technol. 23 (2014) 765–785.
[10] G. Ramírez, S.E. Rodil, H. Arzate, S. Muhl, J.J. Olaya, Niobium based coatings for dental implants, Appl. Surf. Sci. 257 (2011) 2555–2559.
[11] D. Velten, E. Eisenbarth, N. Schanne, J. Breme, Biocompatible Nb_2O_5 thin films prepared by means of the sol–gel process, J. Mater. Sci. Mater. Med. 15 (2004) 457–461.
[12] S. Nagarajan, V. Raman, N. Rajendran, Synthesis and electrochemical characterization of porous niobium oxide coated 316 SS for orthopedic applications, Mater. Chem. Phys. 219 (2010) 363–366.
[13] C.B. da Silveira, A.F. de Oliveira, S.D. de Campos, E.A. de Campos, A.D. Fraporti, Nb_2O_5 coating of glass fibres applied by chemical vapour deposition, Surf. Eng. 28 (2012) 68–72.
[14] G. Ramírez, S.E. Rodil, S. Muhl, D. Turcio-Ortega, J.J. Olaya, M. Rivera, E. Camps, L. Escobar-Alarcón, Amorphous niobium oxide thin films, J. Non-Cryst. Solids 356 (2010) 2714–2721.
[15] R.A. Antunes, M.C.L. de Oliveira, Corrosion processes of physical vapor deposition-coated metallic implants, Crit. Rev. Biomed. Eng. 37 (2009) 425–460.
[16] S. Venkataraj, R. Drese, O. Kappertz, R. Jayavel, M. Wuttig, Characterization of niobium oxide films prepared by reactive DC magnetron sputtering, Phys. Status Solidi A 188 (2001) 1047–1058.
[17] SIMNRA User's Guide, Matej Mayer, Max-Planck-Institut für Plasmaphysik. Available at: www.simnra.com.
[18] M. Serényi, T. Lohner, P. Petrik, Z. Zolnai, Z.E. Horváth, N.Q. Khánh, Characterization of sputtered and annealed niobium oxide films using spectroscopic elipsometry, Rutherford backscattering spectrometry and X-ray diffraction, Thin Solid Films 516 (2008) 8096–8100.
[19] A. Foroughi-Abari, K.C. Cadien, Growth, structure and properties of sputtered niobium oxide thin films, Thin Solid Films 519 (2011) 3068–3073.

[20] K.C. Mohite, Y.B. Khollam, A.B. Mandale, K.R. Patil, M.G. Takwale, Characterization of silicon oxynitride thin films deposited by electron beam physical vapor deposition technique, Mater. Lett. 57 (2003) 4170–4175.
[21] L.A. Dobrzanski, K. Lukaskowicz, A. Zarychta, L. Cunha, Corrosion resistance of multilayer coatings deposited by PVD techniques onto the brass substrate, J. Mater. Process. Technol. 164–165 (2005) 816–821.
[22] E. Akiyama, A. Kawashima, K. Asami, K. Hashimoto, The corrosion behavior of sputter-deposited amorphous Al–Cr–Mo alloys in 1M HCl, Corros. Sci. 38 (1996) 279–292.
[23] C. Liu, Q. Bi, H. Ziegele, A. Leyland, A. Matthews, Structure and corrosion properties of PVD CrN coatings, J. Vacuum Sci. Technol. A 20 (2002) 772–780.
[24] C. Liu, Q. Bi, A. Leyland, A. Matthews, An electrochemical impedance spectroscopy study of the corrosion behaviour of PVD coated steels in 0.5N NaCl aqueous solution: part II. EIS interpretation of corrosion behaviour, Corros. Sci. 45 (2003) 1257–1273.
[25] X.P. Liu, T.L. Zheng, J.P. Xiong, Corrosion resistance of polyuria polyaspartic ester coating in 3.5% NaCl by EIS, Int. J. Electrochem. Sci. 8 (2013) 11588–11595.
[26] A. Xu, F. Zhang, B. Luo, F. Jin, T. Zhang, Investigation the deterioration process of organic coating using changing rate of phase angle at high frequency united to neural network, Int. J. Electrochem. Sci. 8 (2013) 773–779.
[27] E.-S.M. Sherif, J.H. Potgieter, J.D. Comins, L. Cornish, P.A. Olubambi, C.N. Machio, The beneficial effect of ruthenium additions on the passivation of duplex stainless steel corrosion in sodium chloride solutions, Corros. Sci. 51 (2009) 1364–1371.
[28] L. Curkovic, H.O. Curkovic, S. Salopek, M.M. Renjo, S. Segota, Enhancement of corrosion protection of AISI 304 stainless steel by nanostructured sol–gel TiO_2 films, Corros. Sci. 77 (2013) 176–184.
[29] L.J. Zhang, J.J. Fan, Z. Zhang, F.H. Cao, J.Q. Zhang, C.N. Cao, Study on the anodic film formation process of AZ91D magnesium alloy, Electrochim. Acta 52 (2007) 5325–5333.
[30] A.C. Bastos, M.G. Ferreira, A.M. Simões, Corrosion inhibition by chromate and phosphate extracts for iron substrates studied by EIS and SVET, Corros. Sci. 48 (2006) 1500–1512.
[31] V.M.C.A. Oliveira, C. Aguiar, A.M. Vazquez, A. Robin, M.J.R. Barboza, Improving corrosion resistance of Ti–6Al–4V alloy through plasma-assisted PVD deposited nitride coatings, Corros. Sci. 88 (2014) 317–327.
[32] S.P. Mani, A. Srinivasan, N. Rajendran, Effect of nitrides on the corrosion behavior of 316L SS bipolar plates for proton exchange membrane fuel cell (PEMFC), Int. J. Hydrogen Energy 40 (2015) 3359–3369.
[33] Y.H. Yoo, J.H. Hong, J.G. Kim, H.Y. Lee, J.G. Han, Effect of Si addition to CrN coatings on the corrosion resistance of CrN/stainless steel coating/substrate system in a deaerated 3.5 wt.% NaCl solution, Surf. Coat. Technol. 201 (2007) 9518–9523.
[34] N.C. Rosero-Navarro, S.A. Pellice, A. Durán, M. Aparicio, Effects of Ce-containing sol–gel coatings reinforced with SiO_2 nanoparticles on the protection of AA2024, Corros. Sci. 50 (2008) 1283–1291.
[35] M.A. Surmeneva, R.A. Surmenev, Microstructure characterization and corrosion behavior of a nano-hydroxyapatite coating deposited on AZ31 magnesium alloy using radio frequency magnetron sputtering, Vacuum 117 (2015) 60–62.
[36] M. Fouladi, A. Amadeh, Effect of phosphating time and temperature on microstructure and corrosion behavior of magnesium phosphate coating, Electrochim. Acta 106 (2013) 1–12.
[37] J. Barranco, F. Barreras, A. Lozano, M. Maza, Influence of CrN-coating thickness on the corrosion resistance behaviour of aluminium-based bipolar plates, J. Power Sources 196 (2011) 4283–4289.
[38] A.-M. Lazar, W.P. Yespica, S. Marcelin, N. Pébère, D. Samélor, C. Tendero, C. Vahlas, Corrosion protection of 304L stainless steel by chemical vapor deposited alumina coatings, Corros. Sci. 81 (2014) 125–131.
[39] E.-G. Berasategui, R. Bayón, C. Zubizarreta, J. Barriga, R. Barros, R. Martins, E. Fortunato, Corrosion resistance analysis of aluminium-doped zinc ozide layers deposited by pulsed magnetron sputtering, Thin Solid Films (2015), http://dx.doi.org/10.1016/j.tsf.2015.07.010.
[40] Y. Liu, J. Huang, J.B. Claypool, C.E. Castano, M.J. O'Keefe, Structure and corrosion behavior of sputter deposited cerium oxide based coatings with various thickness on Al 2024-T3 alloy substrates, Appl. Surf. Sci. 355 (2015) 805–813.
[41] S. Sonmez, B. Aksakal, B. Dikici, Influence of hydroxyapatite coating thickness and powder particle size on corrosion performance of MA8MA magnesium alloy, J. Alloys Compd. 596 (2014) 125–131.
[42] Y. Zhuang, X. Jiang, A.V. Rogachev, D.G. Piliptsou, B. Ye, G. Liu, T. Zhou, A.S. Rudenkov, Influences of pulse frequency on the structure and anti-corrosion properties of the a-C:Cr films, Appl. Surf. Sci. 351 (2015) 1197–1203.
[43] N. Usha, R. Sivakumar, C. Sanjeeviraja, M. Arivanandhan, Niobium pentoxide (Nb_2O_5) thin films: rf power and substrate temperature induced changes in physical properties, Optik 126 (2015) 1945–1950.
[44] O.D. Coskun, S. Demirel, G. Atak, The effects of heat treatment on optical, structural, electrochromic and bonding properties of Nb_2O_5 thin films, J. Alloys Compd. 648 (2015) 994–1004.
[45] B. Koscielska, A. Winiarski, Structural investigations of nitride Nb_2O_5 and Nb_2O_5–SiO_2 sol–gel derived films, J. Non-Cryst. Solids 354 (2008) 4349–4353.
[46] T. Hong, M. Nagumo, Effect of surface roughness on early stages of pitting corrosion of type 301 stainless steel, Corros. Sci. 39 (1997) 1665–1672.
[47] G. Quartarone, T. Bellomi, A. Zingales, Inhibition of copper corrosion by isatin in aerated 0.5M H_2SO_4, Corros. Sci. 45 (2003) 715–733.
[48] J.O'.M. Bockris, A.K.N. Reddy, Modern Electrochemistry, vol. 2, Plenum Press, New York, 1972, pp. 1265.
[49] S. Ningshen, M. Sakairi, K. Suzuki, S. Ukai, The corrosion resistance and passive film compositions of 12%Cr and 15%Cr oxide dispersion strengthened steels in nitric acid media, Corros. Sci. 78 (2014) 322–334.
[50] B. Díaz, E. Härkonen, J. Swiatowska, V. Maurice, A. Seyeux, P. Marcus, M. Ritala, Low-temperature atomic layer deposition of Al_2O_3 thin coatings for corrosion protection of steel: surface and electrochemical analysis, Corros. Sci. 53 (2011) 2168–2175.
[51] C. Andrade, F. Bolzoni, M. Cabeza, X.R. Nóvoa, M.C. Pérez, Electrochemical Approach to Selected Corrosion and Corrosion Control Studies, in: L. Bonora, F. Deflorian (Eds.), European Federation of Corrosion Pub., No. 28, The Institute of Materials, London, 2000, pp. 332–343.
[52] M.G. Pujar, C.R. Das, S. Thirunavukkarasu, U.K. Mudali, A.K. Bhaduri, J. Brijitta, B.V.R. Tata, Effect of boron addition on pitting corrosion resistance of modified 9Cr–1Mo steel: application of electrochemical noise, Mater. Chem. Phys. 130 (2011) 536–547.
[53] R.M. Fernández-Domene, E. Blasco-Tamarit, D.M. García-García, J. García-Antón, Repassivation of the damage generated by cavitation on UNS N08031 in a LiBr solution by means of electrochemical techniques and confocal laser scanning microscopy, Corros. Sci. 52 (2010) 3453–3464.
[54] R. Leiva-García, J. García-Antón, M.J. Muñoz-Portero, Contribution to the elucidation of corrosion initiation through confocal laser scanning microscopy (CLSM), Corros. Sci. 52 (2010) 2133–2142.
[55] C.Y. Cui, X.G. Cui, Y.K. Zhang, Q. Zhao, J.Z. Lu, J.D. Hu, Y.M. Wang, Microstructure and corrosion behavior of the AISI 304 stainless steel after Nd: YAG pulsed laser surface melting, Surf. Coat. Technol. 206 (2011) 1146–1154.